separations

MDPI

Article

Removal of Azo Dyes Orange II and Reactive Black 5 from Aqueous Solutions by Adsorption on Chitosan Beads Modified with Choline Chloride: Urea Deep Eutectic Solvent and FeO

Óscar Martínez-Rico, Lucía Blanco, Ángeles Domínguez and Begoña González *

Chemical Engineering Department, Universidade de Vigo, 36310 Vigo, Spain; oscar.martinez.rico@uvigo.es (Ó.M.-R.); slblanco@uvigo.es (L.B.); admguez@uvigo.es (Á.D.)
* Correspondence: bgp@uvigo.es

Abstract: The removal of the azo dyes Orange II (OII) and Reactive Black 5 (RB5) from aqueous solutions was studied using three types of adsorbents derived from chitosan: unmodified chitosan beads (un-Ch), chitosan beads tuned with a deep eutectic solvent (DES) composed of choline chloride:urea at a 1:2 molar ratio (Ch-DES), along with FeO nanoparticles added to chitosan and modified with DES (Ch-FeO-DES). Both dyes were effectively removed in 3–4 h when Ch-DES beads were used, at a dye concentration range of 25–50 mg/L. The modification with DES improved the removal efficiency to achieve increases of around 32% for OII and 17% for RB5. The adsorbent dosage and the initial dye concentration influenced the adsorption process. Isotherm adsorption models (Langmuir, Freundlich, and Temkin) and kinetic models (pseudo-first-order, pseudo-second-order, intraparticle diffusion, and Elovich models) were applied to identify the adsorption behavior. The process could be characterized by employing the pseudo-second-order kinetic model and fitting it to the monolayer Langmuir isotherm. The adsorption occurred on a monolayer with no interaction among dye molecules when electrostatic forces would determine the attaching of dye molecules on the adsorbent. OII was efficiently desorbed by an alkaline solution, while RB5 was more strongly attached. The adsorbent could be recycled, after regeneration with an acid solution, for at least 5 reuse cycles while still achieving effective OII removal. Reactivation with a diluted EDTA solution allowed the authors to recycle RB5-attached beads, achieving optimum removal in two further uses.

Keywords: adsorption; chitosan; deep eutectic solvent; protonation; azo dye; textile wastewater remediation; dye removal

Citation: Martínez-Rico, Ó.; Blanco, L.; Domínguez, Á.; González, B. Removal of Azo Dyes Orange II and Reactive Black 5 from Aqueous Solutions by Adsorption on Chitosan Beads Modified with Choline Chloride: Urea Deep Eutectic Solvent and FeO. *Separations* **2023**, *10*, 426. https://doi.org/10.3390/separations10080426

Academic Editor: Paraskevas D. Tzanavaras

Received: 19 June 2023
Revised: 14 July 2023
Accepted: 22 July 2023
Published: 27 July 2023

1. Introduction

Legislation regarding industrial effluents is becoming stricter, triggering increasing research initiatives on the removal of toxic compounds and the prevention of pollutant discharge to the environment [1,2]. Dyes employed by different industrial sectors, such as the textile, paper, cosmetic, printing, and plastic industries, contaminate the aquatic environment [3]. The textile industry is one of the main sources of contaminants to the aquatic environment since large amounts of water are required in the various processes and so effluents containing textile dyes and the additional chemicals required for textile production are generated; as a result, about 10–15% of these dyes are discharged without further treatment [1,3,4]. Textile dyes are among the most concerning pollutants since these water-soluble compounds hinder light penetration and disturb photosynthetic activity in the aquatic environment, affecting organisms throughout the food chain, which eventually causes damage to humans. Small amounts of dyes in water (1 ppm) can be visually detected and can cause public concern and, hence, government attention [2–4].

The textile industry uses about 10,000 types of dyes with varying chemical structures [3,4]. Textile dyes are organic compounds absorbing light in the visible range of the spectrum (380–750 nm). They are conformed by two components: a chromophore group, responsible for

the color, including different functional groups such as –C=C–, –C=O, –N=N– and NO_2, along with auxochromes, which consist of groups containing unshared electron pairs, influencing the color caused by the chromophore. In addition, auxochromes increase the fiber's affinity for color and reduce the dye's water-solubility [4]. There are about 12 different chromophore groups, with the azo type, containing the group –N=N– (azo), being the widest available organic dyes in the market, reaching 60–70% of the total. In addition, they are the most widely used dyes at present in the textile industry, owing to their dyeing capacity and resistance [4,5]. Azoic colorants show one or more azo-bonding structures, linking aromatic rings with functional groups such as –OH or $–SOH_3$ (auxochromes) [6]. Within this group, we can find the colorants Orange II (OII) and Reactive Black 5 (RB5). OII, also known as Betanaphthol Orange, is a monoazoic dye with a sulfonic group in its structure [7] (Figure S1 in the Supplementary Materials). Conversely, RB5 is a diazo compound, since it presents two azo moieties and four sulfonic groups, and aromatic amines are part of its structure [8] (Figure S1).

Hence, an adequate treatment for dye removal from wastewater is required before discharge. Different methodologies, including physical, chemical, and biological approaches have been studied for many years, namely, oxidation, coagulation, adsorption, photocatalysis, aerobic treatment, and membrane filtration, among others [6,9,10]. However, the decoloration of wastewater is a hard task since dyes are synthetic organic compounds that are very difficult to eliminate via conventional methods; they are unaffected by aerobic digestion and are resistant to light, heat, and oxidizing agents. In addition, the complex aromatic structure of azo dyes confers them great stability and makes them difficult to eliminate from effluents [3,9,11]. Adsorption is considered one of the most efficient methods, with a potential application in water and wastewater treatment. This process involves the transfer of the substance molecules to be separated (adsorbate) from the liquid toward the adsorbent (solid phase), leaving the effluent clean [6,9]. Many kinds of adsorbents have been essayed for water depuration, such as peat, silica, chitin, and activated carbon, with the latter being the most widely used and studied. However, the elevated cost of activated carbon production and regeneration has triggered the search for alternative adsorbents [8,12–14]. Cost-effective adsorbents, such as biopolymers, are of great interest at present; among these, chitosan (Ch) is the focus of many adsorption studies.

Chitosan $(C_6H_{11}NO_4)_n$ is the deacetylated form of chitin, a linear polymer of β-(1 4)acetyl-D-glucosamine. This polysaccharide contains the amine and hydroxyl groups, conferring a high availability of active sites that allow an increase in the adsorption capacity of the material. Additionally, these functional groups might generate electrostatic attractions between the chitosan and the solutes, as well as bonding of a physical and/or chemical nature, forming complex structures. In addition, chitosan is abundant in nature, and its non-toxic, hydrophilic character, biocompatibility, and biodegradability make it a polymer of great interest in many fields of application [15]. However, some drawbacks, such as its dissolution in an acid medium, as well as its low porosity, limit its applications as an adsorbent [13,16,17]. The procedure for the gelation of chitosan into hydrogels has been applied to overcome these difficulties, such as the elaboration of beads by dissolving the chitosan powder in an acidic aqueous solution and then dropping it into an alkaline coagulation bath, which causes the chitosan chains to contact and form a three-dimensional network [18]. However, improvements in the stability and efficiency of this biopolymer are needed; therefore, different modifications have been tested, resulting in new physicochemical behaviors of the materials and thereby extending their potential applications [15,19].

Combinations of chitosan with deep eutectic solvents (DES) offer a seldom-explored possibility to obtain eco-friendly, non-toxic, biodegradable, accessible, and cost-effective materials with interesting structural properties [20,21] and improved adsorption capacities to remove pollutants from wastewaters [16,22–24]. DES are compounds that are obtained by combining pure chemicals, which act as hydrogen bond donors and acceptors for given molar proportions. As a result of the establishment of van der Waals forces and hydrogen bonds among the various components, the obtained solvent exhibits a considerably reduced melting point; therefore, it remains liquid at a wide range of temperatures. There are not

many examples in the literature of their potential applications as organic solvent substitutes for the removal of pollutants such as dyes in wastewater [25,26]. Other materials such as iron nanoparticles might provide paramagnetism, a large contact area, and active sites when combined with chitosan and would enable the improvement of the adsorption efficiency and recovery of the materials after the process [17,27].

Therefore, the present work aims to study the modification of chitosan with DES and with FeO nanoparticles for application in the adsorption of azo dyes. Orange II and Reactive Black 5 were selected as model azo dyes. Synthesis of the adsorbents, characterization of the materials, and adsorption experiments were performed. The influence of the adsorbent dose, initial dye concentration, or contact time was also investigated, as well as the adsorption kinetics and isotherms.

2. Materials and Methods

2.1. Chemicals

The chemical reagents used in the present work are listed in Table S1 in the Supplementary Materials. CAS numbers, purities, and suppliers are also indicated. The structures of the relevant compounds are shown in Figure S1 in the Supplementary Materials. Milli-Q water was used to prepare the aqueous solutions. The chitosan molecular weight was 100,000–300,000 and the deacetylation degree was about 84.8%.

2.2. Adsorbents

Three different types of adsorbents based on chitosan beads were prepared, each with its own characteristics: unmodified chitosan beads (un-Ch), chitosan beads tuned with a DES of choline chloride:urea in a molar ratio of 1:2 (Ch-DES), and chitosan beads that incorporate DES and FeO (Ch-FeO-DES). These preparations were carried out following the methodology outlined in our previous study [28]. In brief, to create the un-Ch beads, chitosan was dissolved in 2% (*v*/*v*) acetic acid at a concentration of 40 g/L and allowed to sit for 24 h at a temperature of 333.16 K. The gel solution was then injected into a coagulation bath containing NaOH (2.5 M) using a glass syringe. Afterward, the beads were thoroughly washed and dried at room temperature. For the Ch-DES-modified beads, a portion of the un-Ch beads was separated after washing and then combined with DES in a 1:1 (*w*/*w*) ratio. The mixture was stirred under a vacuum at 333.16 K, washed, and dried. Finally, the Ch-FeO-DES beads were prepared by adding iron oxide nanoparticles to the chitosan gel at a mass ratio of 1:2. The mixture was stirred for 1 h and sonicated for 30 min, then the Ch-FeO beads were formed by adding them to a 2.5 M NaOH solution, following the previously described procedure. After washing, the Ch-FeO beads were mixed with DES for impregnation.

To synthesize the DES solution itself, choline chloride and urea were mixed in a molar ratio of 1:2 and heated at 353.16 K under stirring until the formation of a homogeneous liquid. The FeO particles were prepared through co-precipitation by mixing and heating $FeCl_3 \cdot 6H_2O$ (0.52 M) and $FeCl_2 \cdot 4H_2O$ (0.26 M) at 353.16 K. NaOH (0.1 M) was then added dropwise until the pH reached 10, resulting in the formation of a black precipitate. The precipitate was collected, washed multiple times with water and ethanol, and finally dried at 363.16 K.

2.3. Characterization

Fourier transform infrared (FTIR) was used to obtain the infrared spectra and trace the chemical modifications on the beads after the treatments (impregnation with DES and FeO addition). A Nicolet 6700 device from Thermo Scientific (Waltham, MA, USA), linked to a diamond crystal ATR attachment (Smart Orbit) (Waltham, MA, USA), was employed for attenuated total reflection (ATR) spectroscopy.

The structural modifications on the outer part of the beads were observed using a JEOL JSM 6700F field emission scanning electron microscope (SEM) (Munich, Germany). The TriStar II Plus 3030 system (Micromeritics, Inc.) (Norcross, GA, USA) was used for Barrett–

Joyner–Halenda (BJH) pore volume and size analysis and for Brunauer–Emmett–Teller (BET) surface area analysis.

2.4. Adsorption Experiments

Independent OII and RB5 solutions in concentrations of between 25–150 mg/L were prepared. The pH was not adjusted. Adsorption experiments were carried out with continuous agitation at 350 rpm in an OHAUS ISHD16HDG incubator shaker (Greifensee, Switzerland). First, preliminary tests were performed for the three adsorbents, maintaining the same conditions: 0.025 g of adsorbent, 100 mg/L of dye, for 360 min, and at 298.16 K. The most efficient option was chosen for a more in-depth characterization of its adsorption behavior. Then, different experiments were conducted at varying conditions of the following parameters: adsorbent dosage (0.005–0.035 g), initial concentration of dye (25–150 mg/L), and contact time (15–360 min). The experiments were all performed at a constant temperature (298.16 K). Monitoring of the pH of all the systems at the start and at the end of the experiments was conducted with a HI5221 Hanna pH meter (Bedfordshire, UK). The volume of the solutions was 5 mL throughout the study. A Jasco V-750 UV-VIS spectrometer (Tokyo, Japan) was used to measure the dye concentration, at wavelengths of 483 nm (OII) and 597 nm (RB5). Equations (1)–(3) were used to calculate the amount of dye taken up once equilibrium was achieved (q_e, mg/g), at a given time t (q_t, mg/g), along with the elimination percentage of the dyes:

$$q_e = \frac{V(C_0 - C_e)}{m}; \quad (1)$$

$$q_t = \frac{V(C_0 - C_t)}{m}; \quad (2)$$

$$Dye\ removal\ \% = \frac{C_0 - C_t}{C_0} \times 100. \quad (3)$$

The concentrations (mg/L) of each dye at the start of experimentation, at time t (min), and at equilibrium were, respectively, C_0, C_t, and C_e. The volume of the dye solution is represented by V (L) and the adsorbent dosage by m (g).

Table 1 summarizes the adsorption experiment conditions applied during the study.

Table 1. Overview of the experimental test conditions.

Test	Dye Concentration (mg/L)	Adsorbent	Adsorbent Dosage (g)	Temperature (K)
Adsorbent selection	100	un-Ch Ch-DES Ch-FeO-DES	0.025	298.16
Dosage	100	The best one	0.005, 0.010, 0.015, 0.025, 0.035	298.16
Dye Concentration	25, 50, 100, 150	The best one	The best one	298.16

2.5. Adsorption Isotherm

The Langmuir, Freundlich, and Temkin isotherm models [29–31] have been used to study the affinity, trend, and adsorption mechanism of the dyes OII and RB5 on the selected adsorbent. Equations (S1)–(S4) in the Supplementary Materials represent the mentioned models, respectively.

2.6. Adsorption Kinetics

The kinetic models used to analyze the obtained results were the pseudo-first- and pseudo-second-order kinetic models (Equations (S5) and (S6) in the Supplementary Materials), the Elovich kinetic model (Equation (S7) in the Supplementary Materials), and intraparticle diffusion (Equation (S8) in the Supplementary Materials) [32–34].

2.7. Desorption and Reusability Tests

To evaluate the potential for OII and RB5 desorption, respectively, different alkaline solutions (NaOH 0.1 M, NH_4OH), acid solutions (H_2SO_4 0.1 M, CH_3COOH at 4% and 2%, and EDTA 0.1 M), a salt (NaCl 0.1 M), and the organic solvent DMSO were used. About 0.025 g of the beads used in previous OII and RB5 adsorption tests, respectively, were added into 5 mL of the different solutions; they were stirred for 6 h, after which time the integrity of the adsorbent and the dye desorption were observed. The most efficient desorbing solutions were selected and desorption cycles of varying durations were performed. Equation (4) was used to quantify the desorption.

$$\text{Desorption } (\%) = \frac{C_{des}}{C_{ads}} \times 100 \quad (4)$$

Here, C_{des} is the dye concentration in the desorbed phase, and C_{ads} is the dye concentration in the adsorbed phase. Neutralization of the NaOH solutions containing the desorbed OII was performed before measuring the dye concentration at a wavelength of 483 nm since, in an alkaline medium, the OII dye color changed. Then, the adsorbents were tested for reuse capacity.

Regeneration of the adsorbent was also tested; after (partial) desorption, the beads were washed with water, regenerated (with H_2SO_4 0.1 M or EDTA 0.01 M), washed again with water, and finally reused to adsorb the dyes.

3. Results and Discussion

3.1. Adsorbent Characterization

The morphology and topography of the three types of beads, i.e., un-Ch, Ch-DES, and Ch-FeO-DES, were analyzed via SEM images. The structural changes were explored using surface and porosity analyses (BET surface area analysis and BJH pore size and volume analysis). The infrared spectra of the raw materials and the adsorbents that were obtained via FTIR helped to detect the chemical changes. In this way, the structural and chemical changes generated in the adsorbent by the treatments were explored to achieve a better understanding of the mechanisms underlying their adsorption behavior.

3.1.1. Morphology Study via Scanning Electron Microscopy (SEM)

Figure 1 presents a detailed examination of the surface morphology of the three adsorbents. Scanning electron microscopy (SEM) was employed for sample visualization and a thin layer of gold was sputter-coated prior to analysis. The beads exhibited a spherical-ovoid shape, as shown in Figure S2 in the Supplementary Materials, with a diameter of approximately 0.98 ± 0.11 mm.

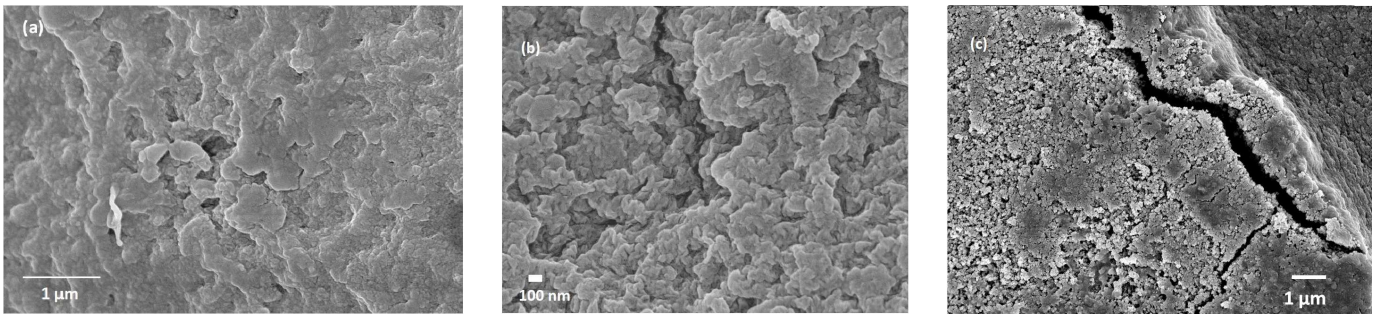

Figure 1. Images of the surface of the adsorbents, obtained via scanning electron microscopy (SEM) with a 5.0 kV acceleration voltage: (**a**) un-Ch (20,000 magnifications, WD 5.9 mm), (**b**) Ch-DES (40,000 magnifications, WD 6.0 mm) and (**c**) Ch-FeO-DES (10,000 magnifications, WD 8.0 mm).

Upon closer observation, the un-Ch beads displayed a relatively smooth surface, featuring minor cavities. In contrast, the Ch-DES beads exhibited areas with a rougher

surface, characterized by an increased presence of cavities and small pores (as seen in Figure 1a,b). Notably, the Ch-FeO-DES beads displayed FeO nanoparticles (as depicted in Figure 1c). These nanoparticles were predominantly visible on the bead's protuberances, while the overall surface appeared mostly smooth (as observed in Figure S2i–l). The rougher surfaces and the greater number of pores observed in the DES and FeO-modified chitosan beads were attributed to the modifications that were made, which included the integration of DES and FeO nanoparticles. These modifications have the potential to enhance the adsorption efficiency of the beads, compared to those consisting solely of chitosan.

3.1.2. BET and BJH Analysis

BET and BJH analysis was conducted to determine the surface area, volume, and pore size of the beads. The results are shown in Table 2.

Table 2. Surface area and porosity analysis of the three adsorbents using Brunauer–Emmett–Teller (BET) and Barrett–Joyner–Halenda (BJH) analysis.

	BET Surface Area (m^2/g)	Pore Volume (cm^3/g)	Pore Size (nm)	Micropore Surface Area (m^2/g)
un-Ch	0.34	3.6×10^{-4}	4.16	0.54
Ch-DES	0.15	1.5×10^{-4}	4.05	0.23
Ch-FeO-DES	0.27	4.3×10^{-4}	6.54	0.142

All the adsorbents showed a very low porosity, with a small pore volume and size. The Ch-FeO-DES beads showed marginally higher values compared to the other two, which could be attributed to the FeO nanoparticles. Nevertheless, their arrangement on the surface of the beads appeared to be limited to isolated spots, as observed in the pictures taken via SEM (Figure S2 in the Supplementary Materials).

3.1.3. Chemical Characterization Using the Fourier Transform Infrared (FTIR) Spectrum

Impregnation with DES and the addition of FeO were carried out and the spectra of each separate compound were obtained. Figure 2 shows the FTIR spectra of DES and the individual components. The main functional groups are listed in Table S2 in the Supplementary Materials. As shown, the formed DES from choline chloride:urea in a molar ratio of 1:2 shows broadened bands at 3500–3000 cm^{-1}, which can be attributed to the hydrogen bonds established between the hydrogen bond acceptor (ChCl) and the donor (urea) [20]. The bands at 3388–3314 cm^{-1} are due to the stretching vibration of the N-H and O-H bonds, while at 3256 and 3187 cm^{-1}, they can be assigned to the N-H stretching vibration. Furthermore, a shift to lower frequencies took place in the band assigned to the C=O stretching vibration of the amide group CONH, shifting from 1674 cm^{-1}, in the urea, to 1660 cm^{-1}, in the DES. Therefore, these changes in the FTIR spectra confirm the presence of interactions among the DES components, leading to a lowering of the melting point.

The spectral changes that can be identified among the adsorbents, as shown in Figure 3, confirm the attachment of the functional groups: in the region of 1500–1700 cm^{-1}, the bands can be assigned to the stretching vibrations of C=O and the bending of N-H bonds of amide (in urea and in chitosan) in the chitosan beads. A new band at 1554 cm^{-1} is present in DES-modified chitosan beads and, together with the band at 1604 cm^{-1}, the intensity of which has grown, can be attributed to the bending of the N-H bonds of the amide and NH_2 groups, coming from the urea in the DES. Furthermore, the band assigned to the stretching of the C=O of the amide I group, seen at 1649 cm^{-1} in un-Ch, moves to 1651 cm^{-1} in the chitosan-DES beads. The area of this peak increases, indicating a possible contribution by another C=O band coming from urea in the DES (Figure 1). These changes occur in both the Ch-DES and Ch-FeO-DES beads. However, the spectra of the Ch-FeO-DES beads do not reflect the incorporated FeO particles, showing the expected bands for magnetite (Fe_3O_4) at 531 cm^{-1}, which can be assigned to the Fe-O stretching vibration (Figure 2). Therefore,

the presence of FeO particles was not evident on the surface of the Ch-FeO-DES beads, as observed via SEM.

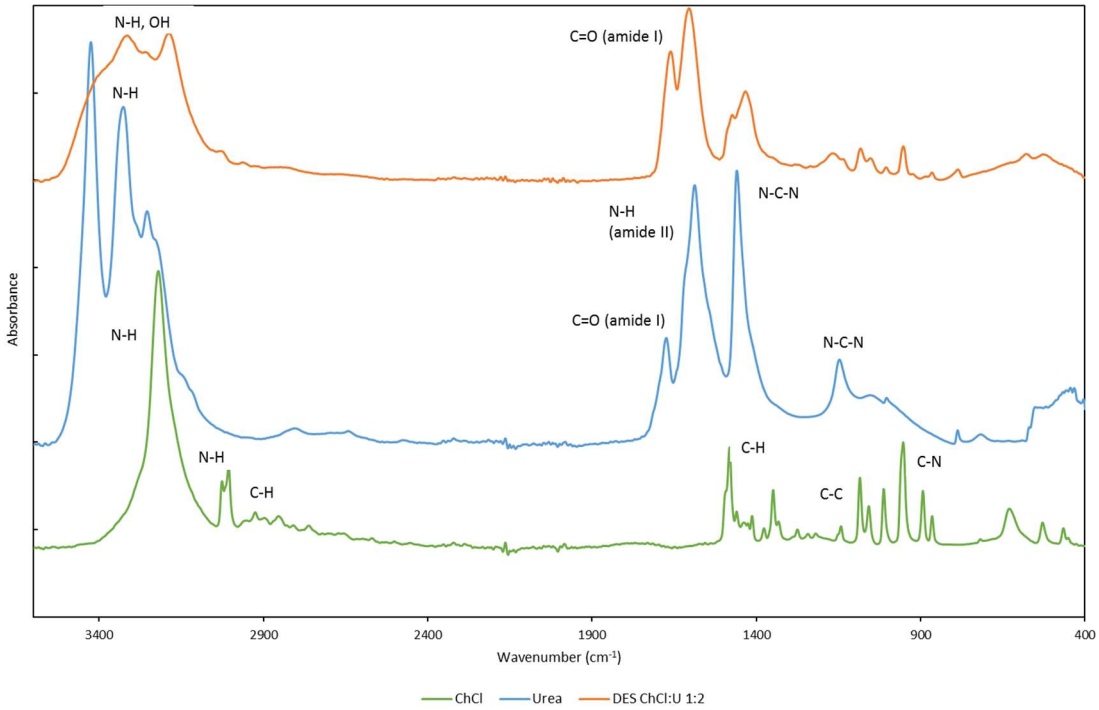

Figure 2. Fourier transform infrared (FTIR) spectra of the DES and their individual components: urea (—), choline chloride (— ChCl), DES choline chloride:urea 1:2 (— DES ChCl:U).

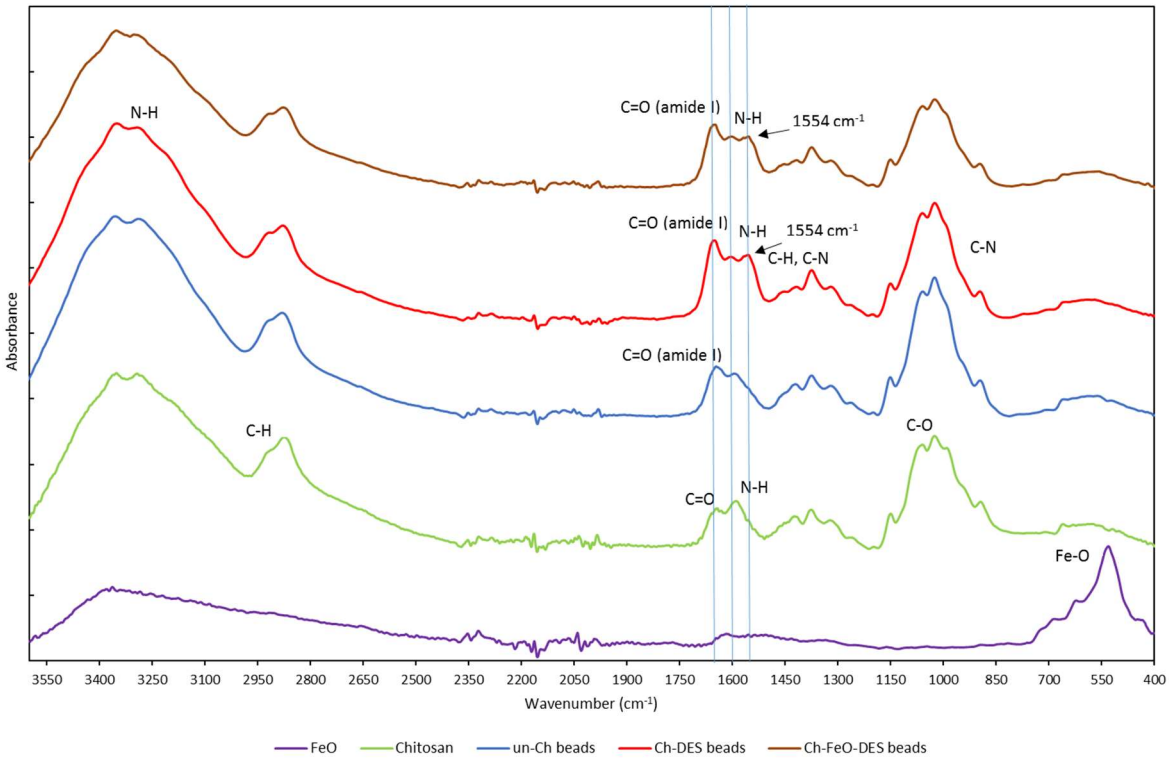

Figure 3. Fourier transform infrared (FTIR) spectra of the reagents: FeO (—), chitosan (—), and the chitosan-based adsorbents, i.e., unmodified chitosan (— un-Ch) beads, DES-modified chitosan (— Ch-DES) beads, and DES-modified chitosan-FeO (— Ch-FeO-DES) beads.

3.2. Preliminary Assays and Selection of the Optimal RB5 Adsorbent

The three types of adsorbents, i.e., un-Ch, Ch-DES, and Ch-FeO-DES, were tested for OII and RB5 adsorption, fixing the following conditions: an initial dye concentration of 100 mg/L and 5 g of adsorbent per liter of solution. Figure 4 shows the obtained results.

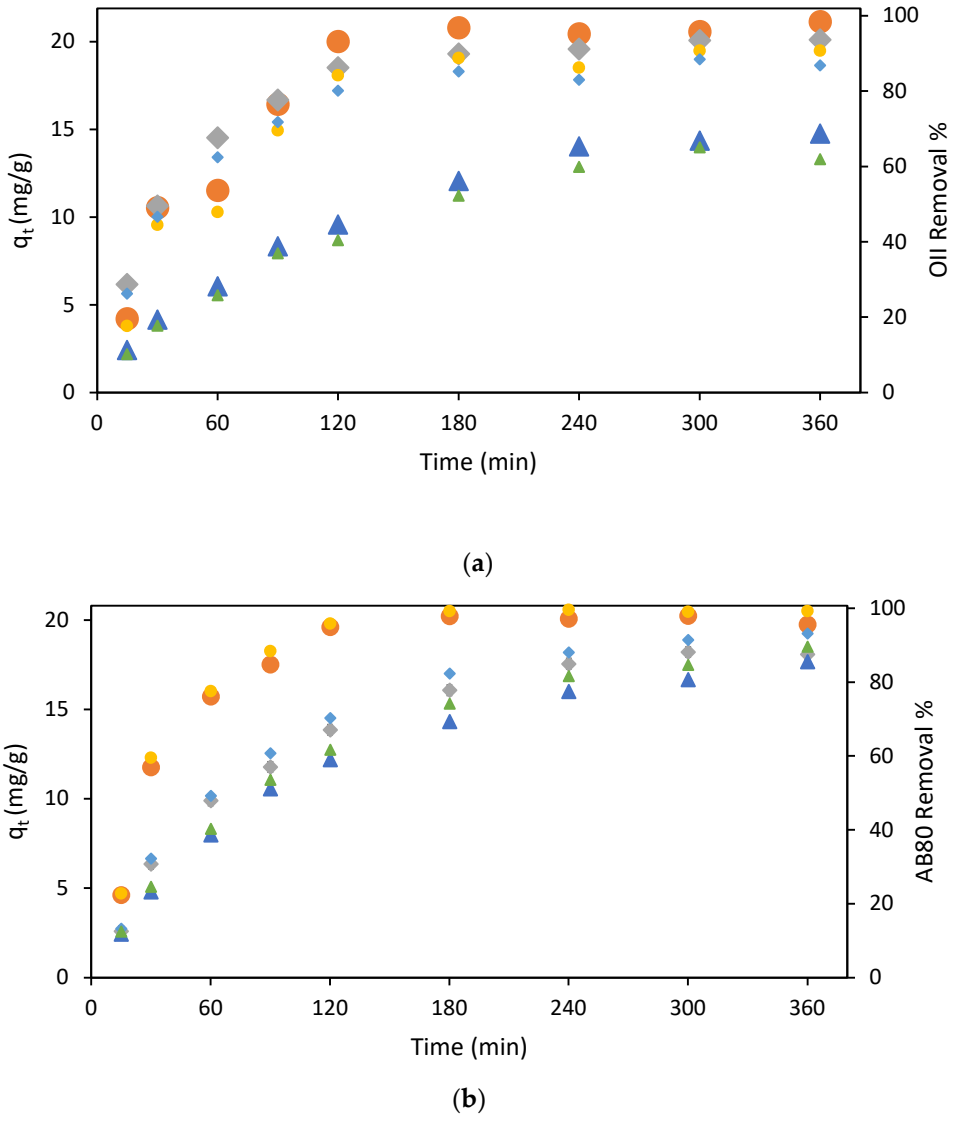

Figure 4. Amount of dye (**a**) OII and (**b**) RB5 adsorbed (q_t), along with time, for the three adsorbents: (▲) un-Ch, (●) Ch-DES, and (◆) Ch-FeO-DES. For the dye's removal from the aqueous solution at 298 K by a ratio adsorbent mass/dye solution volume of 5 g/L: (▲) un-Ch, (●) Ch-DES, and (◆) Ch-FeO-DES.

The Ch-DES and Ch-FeO-DES beads adsorbed both the azo dyes, OII and RB5, at a higher rate than the un-Ch beads. The adsorption capacity and the degree of removal from the solution rise with time, until after 180 min; from that moment on, there is a moderate increase and stabilization until the adsorption capacity achieves 21.1 mg/g OII and 21.0 mg/g RB5 in Ch-DES, with the highest removal percentages being 90.7% for OII and 99.5% for RB5. Ch-DES was the best adsorbent, followed by Ch-FeO-DES, which showed a comparable adsorption efficiency, with a removal rate of 86.8% for OII and 93.6% for RB5, superior to that of un-Ch beads, which showed a rate of 61.9% for OII and 82.4% for RB5 removal. The rapid rises in q_t and in the percentage of removal observed at the beginning of the experiment can be attributed to enhanced surface diffusion and the formation of a film on both types of Ch-DES beads. It is likely that the DES modification of

chitosan beads resulted in a greater quantity of attached functional groups, thereby acting as binding sites.

Therefore, Ch-DES, as the most efficient OII and RB5 adsorbent, was chosen for a more detailed characterization of its adsorptive properties.

3.3. Influences on Adsorption Behaviour

3.3.1. Adsorbent Quantity

The effect of the adsorbent dose on the adsorption capacity and on the OII and RB5 removal percentage was studied to optimize the quantities of beads used in the subsequent experiments. The removal increased with increasing adsorbent mass, until it reached 92% OII and 99% RB5 removal, at a quantity of 0.025 g (in 5 mL of the dye solution) (Figure 5). This increase can be explained by a greater adsorbent surface area and more numerous active functional sites being available for adsorption. Conversely, the adsorption capacity per unit weight decreases with an increasing adsorbent amount; this may be due to a screening effect caused by the accumulation of adsorbent particles and competition among dye molecules for the partially overlapped binding sites [35–37]. Finally, a 0.015 g dose of adsorbent was selected for efficient dye adsorption and removal from the solution.

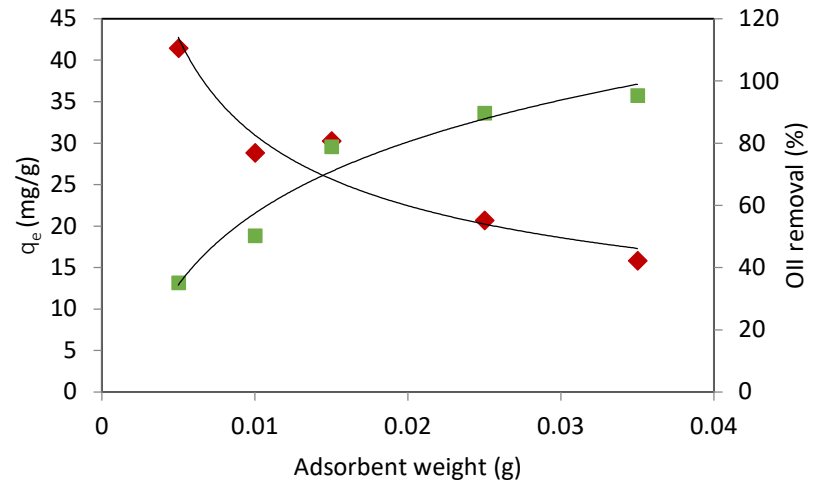

(**a**)

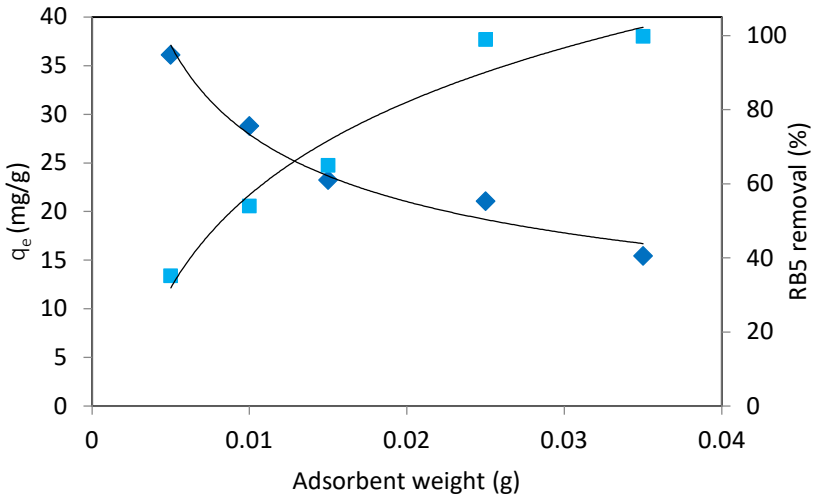

(**b**)

Figure 5. Influence of the varying amounts of the adsorbent Ch-DES beads on the removal efficiency and the amount of dye adsorbed (q_e) for 6 h at 298 K from 5 mL of a 100 mg/L dye solution: (**a**) OII removal (■) and OII amount adsorbed (♦), and (**b**) RB5 removal (■) and RB5 amount adsorbed (♦).

3.3.2. Dye Concentration

The effect of the initial dye concentration on the dye's removal from the solution is shown in Figure 6. During the first step, the removal was rapid, then it proceeded to increase more gradually from 80–180 min, reaching an equilibrium from that moment, at varying times depending on the initial concentration: the lower it was, the greater the removal observed, due to the saturation of active sites at higher dye concentrations. The availability of active sites onn the surface of the Ch-DES bead enabled a higher adsorption rate during the first step of the process; as the process continues and dye molecules occupy the binding sites, adsorption slows down until equilibrium [3,6].

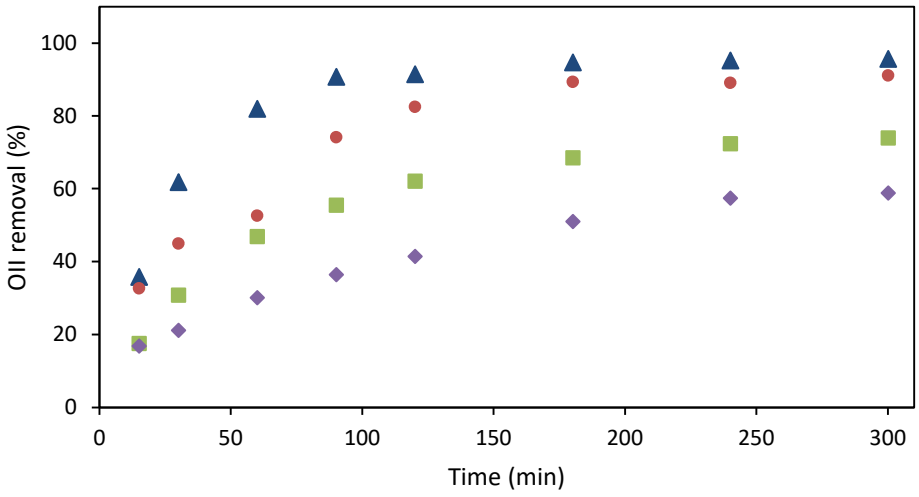

(**a**)

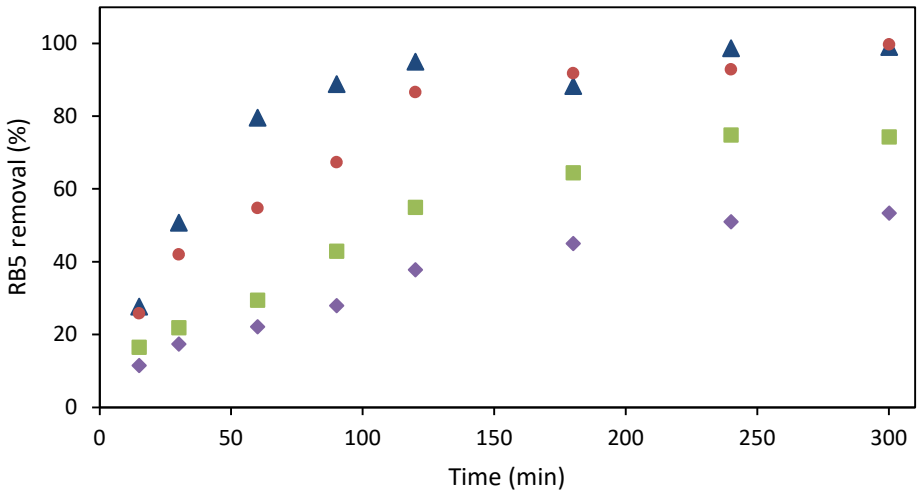

(**b**)

Figure 6. Variation of the percentage of removal of the dyes OII (**a**) and RB5 (**b**) at 298 K for different initial dye concentrations: (▲) 25 mg/L, (●) 50 mg/L, (■) 100 mg/L, (♦) 150 mg/L. A dosage of 0.015 g of Ch-DES beads was used.

At higher initial concentrations, i.e., 100 and 150 mg/L, the adsorption process took more time to achieve equilibrium, about 4–5 h, while at the lowest initial dye concentrations of 25 and 50 mg/L, a duration of 3 h was enough to achieve the maximum values of dye elimination, from the lowest to the highest initial concentrations of 96.7%, 92.1%, 75.0%, and 60.9% for OII, and 99.0%, 99.7%, 74.8%, and 53.3% for RB5.

3.3.3. pH

The interaction between the adsorbate and the adsorbent seems to be of a physical nature. Therefore, the effect of the pH in the beads significantly affects the properties of the beads. Previous work performed by this group [28] studied the point of zero charge (pHpzc) for these materials, obtaining a pH value of 6.98 for Ch-DES. Below that pH, the functional groups on the surface of the beads are protonated, resulting in a net positive charge. Conversely, at a pH of over 6.98, negative charges are predominant on the surface of Ch-DES. It can, therefore, be expected that pHs alter the extraction efficiencies substantially; a more in-depth analysis of this phenomenon is being carried out in this research group and will be the focus of upcoming work.

3.4. Adsorption Isotherms

The experimental data in this study followed typical adsorption curves (as seen in Figure S3 in the Supplementary Materials), with a sharp increase followed by a plateau. These data were also employed to obtain the linear plots of C_e/q_e vs. C_e, log (q_e) vs. log (C_e), and q_e vs. ln (C_e), while R^2 was used to fit the data to the Langmuir (Figure 7), Freundlich, and Temkin isotherms (Figure S4a,b in the Supplementary Materials). The values of the parameters for K_L (the Langmuir constant), K_F (the Freundlich constant), and K_T (the Temkin isotherm constant), while q_m (Langmuir maximum adsorption capacity), n (function of the strength of adsorption), and B (constant related to the heat of adsorption) (defined in the Supplementary Information) were obtained from the linear regressions and are shown in Table 3.

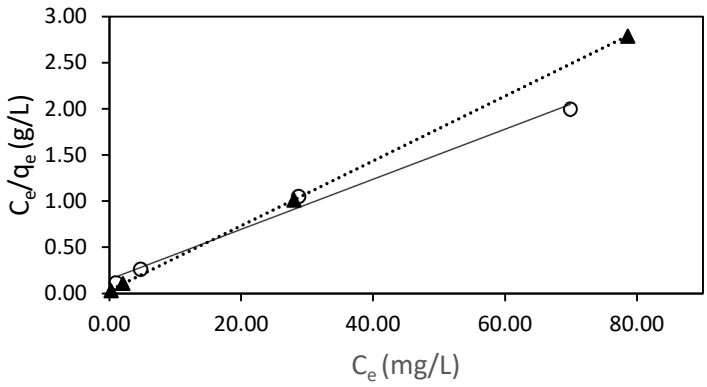

Figure 7. Langmuir plot for the adsorption of OII (○) and RB5 (▲) by 15 mg of Ch-DES beads at 298 K.

Table 3. Isotherm parameters for OII and RB5 adsorption on Ch-DES beads.

	Langmuir Isotherm				Freundlich Isotherm			Temkin Isotherm		
Parameters	q_m **(mg/g)**	K_L **(L/mg)**	R_L	R^2	n	K_F	R^2	B **(J/mol)**	K_T **(L/mol)**	R^2
OII	36.9	177	0.07	0.9901	3	9.5	0.9772	6.0	3.9	0.9920
RB5	28.5	1073	0.01	1.0000	5	13.0	0.9133	3.5	57.0	0.9675

The best fit of the data was achieved using the Langmuir isotherm model. Agreeing with the experimental results, the parameter R_L showed a low value of between 0 and 1 (Table 3). Therefore, it can be assumed that the adsorption occurs via the creation of a monolayer of dye molecules that are uniformly distributed on the adsorbent active sites, with no interactions among the adsorbed molecules [17].

3.5. Adsorption Kinetics

The adsorption of OII and RB5 on Ch-DES beads was studied to determine the adsorption kinetic model that best explained the experimental results. The pseudo-first-order,

pseudo-second-order (Figure 8), intra-particle diffusion (Weber–Morris), and Elovich kinetic models were selected to represent the experimental data. Linear plots of ln ($q_e - q_t$) vs. t, t/q_t vs. t, q_t vs. ln (t), and q_t vs. $t^{1/2}$, in that order, were represented to obtain the parameters. The values for k_1, k_2, k_3, q_e, I, β, and α from the different models (defined in the Supplementary Information) were obtained from the linear plots, and are shown in Table 4 with the corresponding R^2 values.

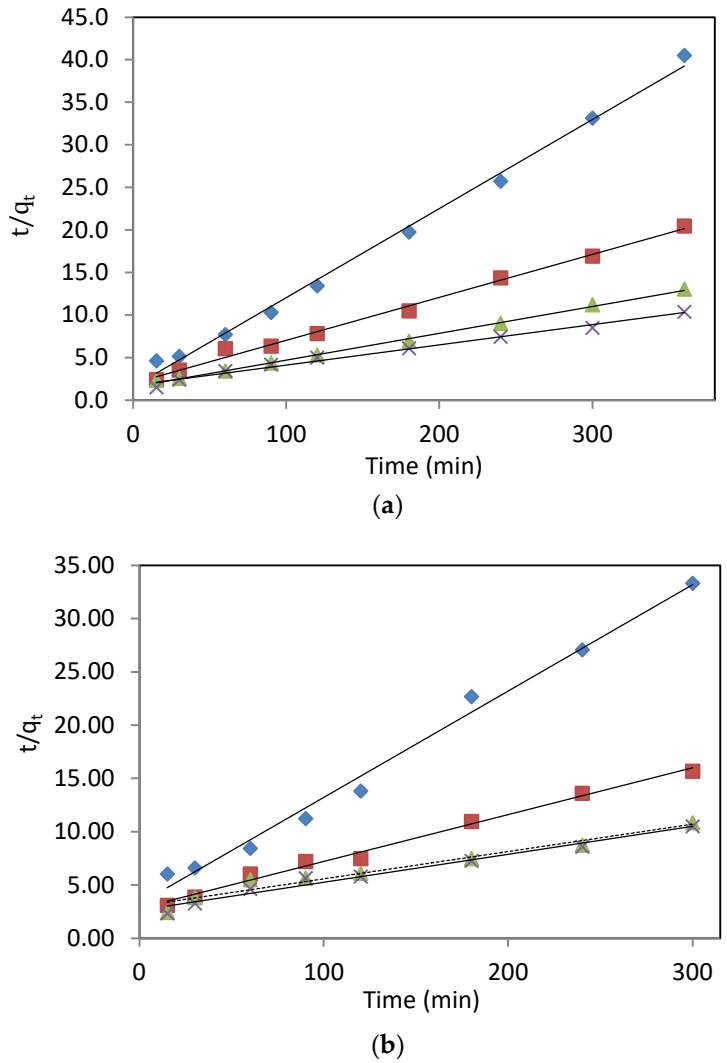

Figure 8. Pseudo-second-order adsorption kinetics of OII (**a**) and RB5 (**b**) at 298 K by 15 mg of Ch-DES beads, at several dye initial concentrations: (♦) 25 mg/L, (■) 50 mg/L, and (▲) 100 mg/L, (×) 150 mg/L.

The pseudo-second-order model was the best-fitting model, as shown by the linear fit (Figure 8) and regression coefficient values (Table 4) for both dyes. There was also an agreement between the calculated and experimental values for q_e. This means that the chemical adsorption determines the process.

Therefore, the rate of OII and RB5 adsorption on Ch-DES beads was dependent on the binding sites and the dye solution concentration. Surface monolayer adsorption was the main mechanism, achieved via the attachment of the dye molecules to the adsorbent surface. This bonding is probably due to electrostatic interactions among the amino groups in the Ch-DES beads and the sulfonate groups in the dyes [17,28].

Table 4. Parameters of the kinetic models for OII and RB5 adsorption by Ch-DES beads.

Dye	**OII**				**RB5**			
Concentration (mg/L)	25	50	100	150	25	50	100	150
q_e, exp (mg/g)	8.98	17.66	27.17	34.97	8.93	18.35	27.49	28.16
Pseudo-first-order kinetic model								
k_1 (1/min)	97.0×10^{-3}	15.9×10^{-3}	12.6×10^{-3}	13.5×10^{-3}	15.7×10^{-3}	11.0×10^{-3}	21.1×10^{-3}	16.8×10^{-3}
q_e (mg/g)	1.50	15.51	19.53	41.41	5.30	14.19	53.37	39.64
R^2	0.4403	0.9393	0.9435	0.9424	0.8387	0.4790	0.8983	0.9322
Pseudo-second-order kinetic model								
k_2 (mg/(g min))	6.9×10^{-3}	1.3×10^{-3}	0.6×10^{-3}	0.3×10^{-3}	3.1×10^{-3}	0.7×10^{-3}	0.2×10^{-3}	0.3×10^{-3}
q_e (mg/g)	9.55	19.80	31.75	42.02	10.01	22.73	38.91	38.17
R^2	0.9952	0.9942	0.9978	0.9879	0.9897	0.9908	0.9572	0.9765
Elovich kinetic model								
β (g/mg)	0.582	0.254	0.146	0.116	0.468	0.206	0.125	0.125
α (mg/(g min))	1.63	1.24	1.36	1.36	2.14	0.80	0.79	0.89
R^2	0.8175	0.9499	0.9780	0.9715	0.8929	0.9760	0.9440	0.9598
Intraparticle diffusion kinetic model								
k_3 (mg/(g $min^{1/2}$))	0.307	0.772	1.324	1.774	0.428	1.048	1.784	1.769
I	4.38	4.90	5.54	3.89	2.59	2.03	−1.26	−0.27
R^2	0.6237	0.8737	0.8761	0.9772	0.7470	0.9468	0.9761	0.982

3.6. Reusability of the Adsorbent

3.6.1. Desorption

Alkaline solution NaOH 0.1 M was employed to desorb the dyes from the beads after adsorption. OII desorption was achieved, with a total desorption value of 81.7% after 3 cycles (6 h per cycle) (Figure 9). Conversely, RB5 desorption was negligible when the NaOH solution was used. Another alkaline solvent, NH_4OH, and different solvents, such as DMSO, along with acid solutions (0.1 M sulfuric acid, 2 and 4% acetic acid) were essayed to elute RB5, without achieving desorption. Acetic acid even dissolved the beads. Finally, a 0.1 M solution of EDTA desorbed a small proportion (5.9%) of the RB5 dye adsorbed on the Ch-DES beads. However, the structure of the beads was altered after the treatment since they had swollen and opened up.

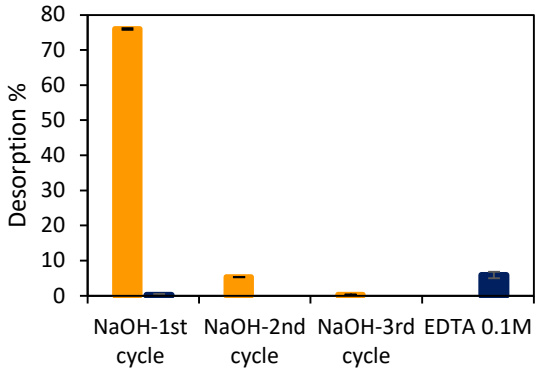

Figure 9. Desorption of OII (■) and RB5 (■) by applying NaOH 0.1 M or EDTA 0.1 M (298 K, 350 rpm, 6 h contact time).

The OH^- ions probably competed and displaced the anionic OII adsorbed molecules from the adsorbent surface, as reported by Wu et al. (2019) [18]. Conversely, the adsorption of RB5 onto the Ch-DES beads seems stronger, possibly helped by the four sulfonate groups, in contrast to the OII unique sulfonate group (Figure S1 in the Supplementary Materials), or via additional interactions.

3.6.2. Reuse of Ch-DES Beads

The adsorbents treated for desorption were tested for reuse. Previously, it was reported that the reuse of NaOH-desorbed beads did not allow efficient dye removal [28]; therefore, the NaOH-OII-desorbed beads were regenerated with 0.1 M sulfuric acid and thoroughly washed with water. Then, after drying, they were reused 5 times for OII adsorption. The results obtained (see Figure 10) showed enhanced performance as an OII adsorbent after the desorption-regeneration treatment, achieving 96% removal, in contrast to the initially achieved value of 79% before regeneration. The adsorption capacity increased by about 8% of the initial adsorption capacity value (30.3 vs. 32.3 mg OII/g, on average). After the second use, neither desorption nor regeneration was applied, and the beads were only water-washed and dried. They maintained their OII efficiency removal for at least 5 successive uses.

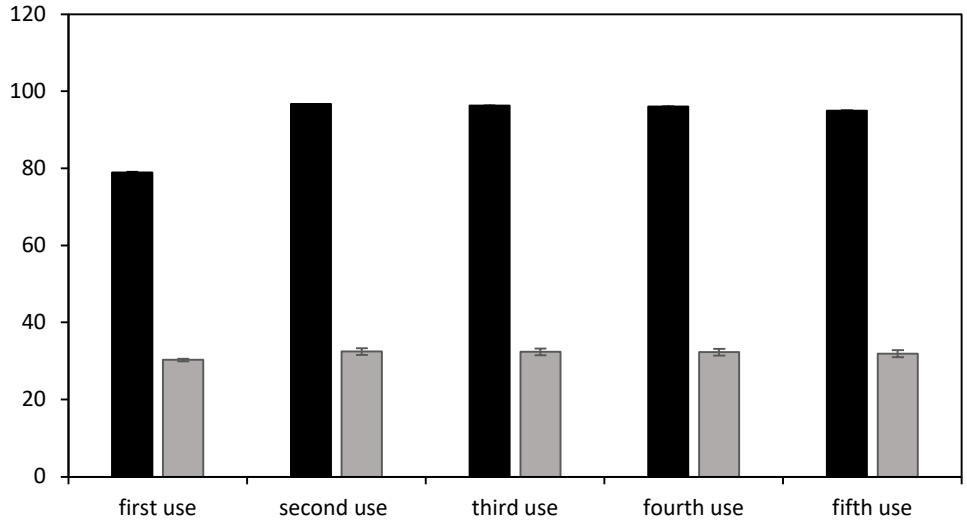

Figure 10. Reusability of the NaOH-OII-desorbed and acid-regenerated Ch-DES beads for OII adsorption. The adsorption tests were carried out at 100 mg/L initial OII concentration, 350 rpm, 15 mg of adsorbent, and 6 h contact time: (■) dye removal % and (▒) adsorption (mg/g).

Subsequently, reuse of the RB5-adsorbed beads was carried out after treatment with a lower EDTA concentration (0.01 M), to diminish possible structural changes. The results are shown in Figure 11. Higher RB5 adsorption performance after the EDTA treatment was achieved, with 99.8% removal in only 4 h, in contrast to the initially achieved value of 64.9%, on average, after 6 h. The adsorption capacity increased to about 32% of the initial adsorption capacity value (34.4 vs. 23.2 mg RB5/g, on average). After the second use, the beads were only water-washed and showed a similar RB5 efficiency removal and adsorption capacity when compared to the first use. However, during the third use, the efficiency dropped (Figure 11), and partial disintegration of the beads was observed. EDTA has been used as a chelating agent for the removal of heavy metals via a metal-complexing mechanism, as well as acting as a crosslinker in adsorbents used for binding metals and dyes [38]. This compound had probably attached to the adsorbent surface and helped in RB5 dye removal from the solution, also causing modifications to the bead's structure, which finally collapsed.

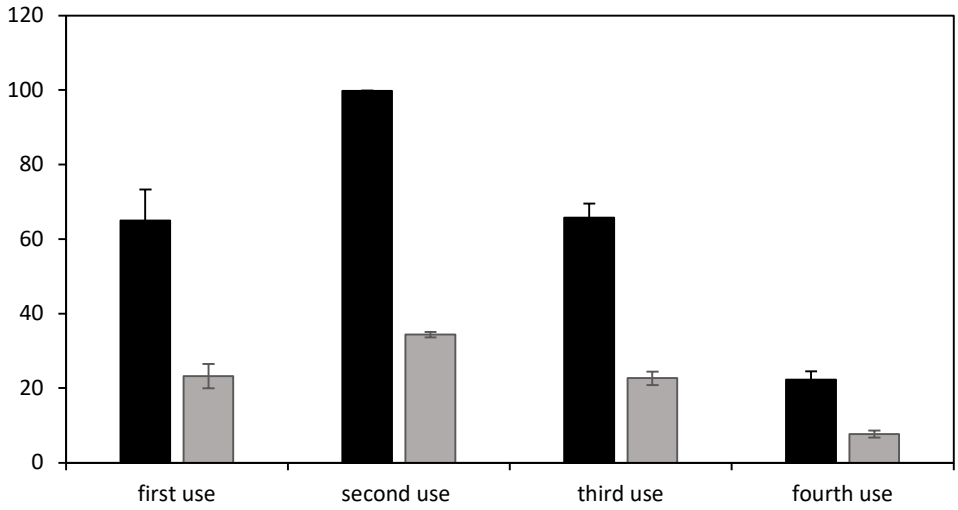

Figure 11. Reusability of the adsorbed RB5-Ch-DES beads after treatment with 0.01 M EDTA for RB5 adsorption. The adsorption tests were carried out at 100 mg/L initial RB5 concentration, 350 rpm, 15 mg of adsorbent, and 4 h contact time: (■) dye removal % and (▒) adsorption (mg/g).

3.7. Rationalization of the Adsorption Mechanism

The adsorption of the azo dyes OII and RB5 was confirmed via FTIR spectroscopy (Figure S5 in the Supplementary Materials), wherein the characteristic bands of the dyes and the adsorbent are shown to be present. The beads show some differences after adsorption in the stretching vibration of the C-H groups (2848–2963 cm^{-1}) and in the stretching vibration of the N-H and O-H groups (about 3300 cm^{-1}). The intensity of the adsorption bands in the range of 1300 to 1680 cm^{-1} decreased, suggesting that possible interactions between the dye molecules and the functional groups, such as -NH_2, of the beads occurred during the adsorption process [18], giving rise to incorporation of the dye into the beads. Since no obvious new peaks appeared and the bands of the adsorbed dyes were slightly shifted with respect to the OII and RB5 dyes, the adsorbent–pollutant interaction must essentially be of a physical nature [6].

The improved adsorption capacity of the Ch-DES beads compared to un-Ch beads is probably due to an increase in the functional groups that act as binding sites for dyes, such as the C=O and NH_2 groups coming from urea in the DES, as was confirmed via FTIR analysis. The electrostatic interactions among the amino groups and the sulfonate groups in the dyes would explain the obtained results, including the stronger attachment of RB5, which did not elute with NaOH, which was possibly helped by the four sulfonate groups present in the dye structure. In addition, the amino group in the RB5 molecule (Figure S1 in the Supplementary Materials) could also be attached to the C=O–O^- groups in the beads [39,40], explaining the stronger union of this dye to the Ch-DES beads, and its behavior against EDTA molecules, the structure of which has four carboxylic acid groups and two amine groups.

4. Conclusions

The adsorption of the azo dyes OII and RB5 was improved when chitosan beads were modified with choline chloride:urea DES. At initial dye concentrations of 50 mg/L and under, the practically total removal of both dyes was achieved in a few hours. The pseudo-second-order kinetic model and the monolayer Langmuir isotherm can be used to explain the process. The adsorption seems to occur on a monolayer, with no interaction among dye molecules, and electrostatic forces determine the attachment of dye molecules to the adsorbent; additional forces seem to bind RB5 more strongly to the Ch-DES beads than OII. Interestingly, the adsorbent could be recycled after use in OII removal from a solution, and desorption, regeneration, and reuse were possible for at least 5 times more, demonstrating an excellent potential for OII removal. Regeneration with diluted sulfuric acid was needed

for efficient adsorbent reutilization. This finding highlights an opportunity for the industrial application and cost-effective use of this adsorbent, as it can also be used for other dyes, offering the potential to foster the advancement of eco-friendly and sustainable approaches for water remediation, thereby promoting the principles of the circular economy.

Supplementary Materials: The following supporting information can be downloaded at: https://www.mdpi.com/article/10.3390/separations10080426/s1. Figure S1: Structures of the dyes RB5 (a) and OII (b), the proposed structure for choline chloride:urea 1:2 eutectic mixture (Longo and Craveiro, 2018) (c), and chitosan structure (d); Table S1: Compounds used in this study and specifications—(chemical name, supplier, purity provided by supplier and CAS number); Figure S2: Images of the surface of the adsorbents obtained by scanning electron microscopy (SEM): (a–d) unmodified chitosan beads (un-Ch), (e–h) chitosan-DES beads (Ch-DES) and (i–l) chitosan-FeO-DES beads (Ch-FeO-DES); Table S2: the main functional groups observed in the individual components of un-Ch and Ch-DES beads by FTIR analysis; Figure S3. Adsorption isotherms for the adsorption of OII (○) and RB5 (▲) by 15 mg of Ch-DES beads at 298 K; Figure S4: Freundlich (a) and Temkin (b) isotherms for the adsorption of OII (♦) and RB5 (■) by 15 mg of Ch-DES beads at 298 K; Figure S5: Fourier transform infrared (FTIR) spectra obtained after the adsorption of the dye OII onto DES-modified chitosan (— Ch-DES-OII) beads and the dye RB5 onto DES-modified chitosan (— Ch-DES-RB5) beads compared to the spectra of the adsorbent before adsorption (— Ch-DES beads), and the spectra of the dyes OII (—) and RB5 (—).

Author Contributions: Conceptualization, L.B., Ó.M.-R., Á.D. and B.G.; methodology, L.B. and Ó.M.-R.; validation, B.G. and Á.D.; investigation, L.B. and Ó.M.-R.; resources, B.G. and Á.D.; data curation, L.B. and Ó.M.-R.; writing—original draft preparation, L.B. and Ó.M.-R.; writing—review and editing, L.B., Ó.M.-R., Á.D. and B.G.; supervision, B.G. and Á.D.; project administration, B.G. and Á.D.; funding acquisition, B.G. and Á.D. All authors have read and agreed to the published version of the manuscript.

Funding: This work was funded by Agencia Estatal de Investigación (Spain) (PID2019-107728RB-I00/AEI/10.13039/501100011033) and Xunta de Galicia (GPC-ED431B 2020/08).

Data Availability Statement: The data presented in this study are available in the manuscript and Supplementary Materials.

Acknowledgments: Authors would like to thank Estefanía López and Marcin Grzelczak, for their valuable contributions on Fourier Transform Infrared Spectroscopy and Scanning Electron Microscopy, respectively, performed at CACTI facilities of Universidade de Vigo, and Alberto Núñez, on Brunauer-Emmett-Teller (BET) and Barrett-Joyner-Halenda (BJH) analyses performed at SAI facilities of Universidade da Coruña.

Conflicts of Interest: The authors declare no conflict of interest.

References

1. Vallvé, M.M.V. Eliminación del Color de las Aguas Residuales Procedentes de la Tintura con Colorantes Reactivos. Doctoral Thesis, Universitat Politècnica de Catalunya, Barcelona, Spain, 2015.
2. Slokar, Y.; Le Marechal, A.M. Methods of decoloration of textile wastewaters. *Dye. Pigment.* **1998**, *37*, 335–356. [CrossRef]
3. Hamzeh, Y.; Ashori, A.; Azadeh, E.; Abdulkhani, A. Removal of Acid Orange 7 and Remazol Black 5 reactive dyes from aqueous solutions using a novel biosorbent. *Mater. Sci. Eng. C* **2012**, *32*, 1394–1400. [CrossRef] [PubMed]
4. Sharma, J.; Sharma, S.; Soni, V. Classification and impact of synthetic textile dyes on Aquatic Flora: A review. *Reg. Stud. Mar. Sci.* **2021**, *45*, 101802. [CrossRef]
5. De Moraes, S.G.; Freire, R.S.; Durán, N. Degradation and toxicity reduction of textile effluent by combined photocatalytic and ozonation processes. *Chemosphere* **2000**, *40*, 369–373. [CrossRef] [PubMed]
6. García, E.R.; Medina, R.L.; Lozano, M.M.; Pérez, I.H.; Valero, M.J.; Franco, A.M.M. Adsorption of Azo-Dye Orange II from Aqueous Solutions Using a Metal-Organic Framework Material: Iron-Benzenetricarboxylate. *Materials* **2014**, *7*, 8037–8057. [CrossRef]
7. PubChem; NIH; National Library of Medicine; National Center for Biotechnology Information. Acid Orange 7. Compound Summary. Available online: https://pubchem.ncbi.nlm.nih.gov/compound/Acid-orange-7 (accessed on 17 March 2023).
8. Cueva, E.M. Reducción de la Concentración de Colorante Negro Reactivo 5 en Agua Mediante el Uso de las Micro Nanoburbujas de Ozono-Aire Escala Laboratorio. 2017. Available online: https://hdl.handle.net/20.500.12692/13412 (accessed on 14 March 2023).

9. Anjaneyulu, Y.; Chary, N.S.; Raj, D.S.S. Decolourization of Industrial Effluents—Available Methods and Emerging Technologies—A Review. *Rev. Environ. Sci. Bio Technol.* **2005**, *4*, 245–273. [CrossRef]
10. Patel, R.; Suresh, S. Kinetic and equilibrium studies on the biosorption of reactive black 5 dye by Aspergillus foetidus. *Bioresour. Technol.* **2008**, *99*, 51–58. [CrossRef]
11. Crini, G. Non-conventional low-cost adsorbents for dye removal: A review. *Bioresour. Technol.* **2006**, *97*, 1061–1085. [CrossRef]
12. Figueroa, D.; Moreno, A.; Hormaza, A.; Sc, M.; Asociado, P. Equilibrio, termodinámica y modelos cinéticos en la adsorción de Rojo 40 sobre tuza de maíz. *Rev. Ing. Univ. Medellín* **2015**, *14*, 105–120. [CrossRef]
13. Chiou, M.-S.; Ho, P.-Y.; Li, H.-Y. Adsorption of anionic dyes in acid solutions using chemically cross-linked chitosan beads. *Dye. Pigment.* **2004**, *60*, 69–84. [CrossRef]
14. Ouachtak, H.; El Guerdaoui, A.; El Haouti, R.; Haounati, R.; Ighnih, H.; Toubi, Y.; Alakhras, F.; Rehman, R.; Hafid, N.; Addi, A.A.; et al. Combined molecular dynamics simulations and experimental studies of the removal of cationic dyes on the eco-friendly adsorbent of activated carbon decorated montmorillonite Mt@AC. *RSC Adv.* **2023**, *13*, 5027–5044. [CrossRef] [PubMed]
15. Da Silva Alves, D.C.; Healy, B.; Pinto, L.A.D.A.; Cadaval, T.R.S., Jr.; Breslin, C.B. Recent Developments in Chitosan-Based Adsorbents for the Removal of Pollutants from Aqueous Environments. *Molecules* **2021**, *26*, 594. [CrossRef] [PubMed]
16. Sadiq, A.C.; Rahim, N.Y.; Suah, F.B.M. Adsorption and desorption of malachite green by using chitosan-deep eutectic solvents beads. *Int. J. Biol. Macromol.* **2020**, *164*, 3965–3973. [CrossRef] [PubMed]
17. Patiño-Ruiz, D.A.; De Ávila, G.; Alarcón-Suesca, C.; González-Delgado, D.; Herrera, A. Ionic Cross-Linking Fabrication of Chitosan-Based Beads Modified with FeO and TiO_2 Nanoparticles: Adsorption Mechanism toward Naphthalene Removal in Seawater from Cartagena Bay Area. *ACS Omega* **2020**, *5*, 26463–26475. [CrossRef] [PubMed]
18. Wu, M.; Chen, W.; Mao, Q.; Bai, Y.; Ma, H. Facile synthesis of chitosan/gelatin filled with graphene bead adsorbent for orange II removal. *Chem. Eng. Res. Des.* **2019**, *144*, 35–46. [CrossRef]
19. Sirajudheen, P.; Poovathumkuzhi, N.C.; Vigneshwaran, S.; Chelaveettil, B.M.; Meenakshi, S. Applications of chitin and chitosan based biomaterials for the adsorptive removal of textile dyes from water—A comprehensive review. *Carbohydr. Polym.* **2021**, *273*, 118604. [CrossRef]
20. Jakubowska, E.; Gierszewska, M.; Nowaczyk, J.; Olewnik-Kruszkowska, E. Physicochemical and storage properties of chitosan-based films plasticized with deep eutectic solvent. *Food Hydrocoll.* **2020**, *108*, 106007. [CrossRef]
21. Pontillo, A.R.N.; Koutsoukos, S.; Welton, T.; Detsi, A. Investigation of the influence of natural deep eutectic solvents (NaDES) in the properties of chitosan-stabilised films. *Mater. Adv.* **2021**, *2*, 3954–3964. [CrossRef]
22. Dai, Y.; Row, K.H. Magnetic chitosan functionalized with β-cyclodextrin as ultrasound-assisted extraction adsorbents for the removal of methyl orange in wastewater coupled with high-performance liquid chromatography. *J. Sep. Sci.* **2018**, *41*, 3397–3403. [CrossRef]
23. Lawal, I.A.; Dolla, T.H.; Pruessner, K.; Ndungu, P. Synthesis and characterization of deep eutectic solvent functionalized CNT/$ZnCo_2O_4$ nanostructure: Kinetics, isotherm and regenerative studies on Eosin Y adsorption. *J. Environ. Chem. Eng.* **2018**, *7*, 102877. [CrossRef]
24. Li, G.; Row, K.H. Deep eutectic solvents skeleton typed molecularly imprinted chitosan microsphere coated magnetic graphene oxide for solid-phase microextraction of chlorophenols from environmental water. *J. Sep. Sci.* **2019**, *43*, 1063–1070. [CrossRef]
25. Blanco, L.V.; Sas, O.G.; Sánchez, P.B.; Santiago, D.; de Prado, B.G. Congo red recovery from water using green extraction solvents. *Water Resour. Ind.* **2022**, *27*, 100170. [CrossRef]
26. Villar, L.; Martínez-Rico, Ó.; Asla, A.; Domínguez, Á.; González, B. Testing Thymol-Based DES for the Elimination of 11 Textile Dyes from Water. *Separations* **2022**, *9*, 442. [CrossRef]
27. Starbird-Pérez, R.; Montero-Campos, V. Synthesis of magnetic iron oxide nanoparticles toward arsenic removal from drinking water. *Rev. Tecnol. Marcha* **2015**, *28*, 45. [CrossRef]
28. Blanco, L.; Martínez-Rico, O.; Domínguez, Á.; González, B. Removal of Acid Blue 80 from aqueous solutions using chitosan-based beads modified with choline chloride:urea Deep Eutectic Solvent and FeO. *Water Resour. Ind.* **2023**, *29*, 100195. [CrossRef]
29. Langmuir, I. The adsorption of gases on plane surfaces of glass, mica and platinum. *J. Am. Chem. Soc.* **1918**, *40*, 1361–1403. [CrossRef]
30. Freundlich, H.M.F. Über die Adsorption in Lösungen. *Z. Phys. Chem.* **1907**, *57U*, 385–470. [CrossRef]
31. Temkin, M.I.; Pyzhev, V. Kinetic of Ammonia Synthesis on Promoted Iron Catalysts. *J. Phys. Chem. USSR* **1939**, *13*, 851–857.
32. Soliman, N.K.; Moustafa, A.F.; El-Mageed, H.R.A.; Abdel-Gawad, O.F.; Elkady, E.T.; Ahmed, S.A.; Mohamed, H.S. Experimentally and theoretically approaches for disperse red 60 dye adsorption on novel quaternary nanocomposites. *Sci. Rep.* **2021**, *11*, 10000. [CrossRef]
33. Wu, F.-C.; Tseng, R.-L.; Juang, R.-S. Initial behavior of intraparticle diffusion model used in the description of adsorption kinetics. *Chem. Eng. J.* **2009**, *153*, 1–8. [CrossRef]
34. Weber, W.J., Jr.; Morris, J.C. Kinetics of Adsorption on Carbon from Solution. *J. Sanit. Eng. Div.* **1963**, *89*, 31–59. [CrossRef]
35. Hamd, A.; Rady, D.; Shaban, M.; Elsayed, K.N.M.; Al Mohamadi, H.; Elzanaty, A.M.; Ahmed, S.A.; El-Sayed, R.; Soliman, N.K. Application of Nano Bio-clay Composite in a Scaling-up Study for Wastewater Treatment. *Biointerface Res. Appl. Chem.* **2021**, *12*, 6393–6414. [CrossRef]

36. Dryaz, A.R.; Shaban, M.; AlMohamadi, H.; Abu Al-Ola, K.A.; Hamd, A.; Soliman, N.K.; Ahmed, S.A. Design, characterization, and adsorption properties of Padina gymnospora/zeolite nanocomposite for Congo red dye removal from wastewater. *Sci. Rep.* **2021**, *11*, 21058. [CrossRef] [PubMed]
37. Mohamed, H.S.; El-Mageed, H.R.A.; Ali, H.S.; Mahmoud, T.R.; Ahmed, S.A.; Soliman, N.K. Adsorption of Mn^{+7} ions on chitosan/cellulose composite: Experimentally and theoretically approaches. *J. Dispers. Sci. Technol.* **2021**, *43*, 1525–1542. [CrossRef]
38. Aramesh, N.; Bagheri, A.R.; Bilal, M. Chitosan-based hybrid materials for adsorptive removal of dyes and underlying interaction mechanisms. *Int. J. Biol. Macromol.* **2021**, *183*, 399–422. [CrossRef] [PubMed]
39. Verma, M.; Lee, I.; Hong, Y.; Kumar, V.; Kim, H. Multifunctional β-Cyclodextrin-EDTA-Chitosan polymer adsorbent synthesis for simultaneous removal of heavy metals and organic dyes from wastewater. *Environ. Pollut.* **2022**, *292*, 118447. [CrossRef]
40. Chen, B.; Zhao, H.; Chen, S.; Long, F.; Huang, B.; Yang, B.; Pan, X. A magnetically recyclable chitosan composite adsorbent functionalized with EDTA for simultaneous capture of anionic dye and heavy metals in complex wastewater. *Chem. Eng. J.* **2018**, *356*, 69–80. [CrossRef]